Autonomous Formation Flying for the PRISMA Mission

Eberhard Gill,* Simone D'Amico,* and Oliver Montenbruck*
DLR, German Aerospace Center, 82234 Wessling, Germany

PRISMA is a technology demonstration mission for satellite formation flying and in-orbit servicing. The space segment comprises the fully maneuverable Main minisatellite and the smaller Target satellite in a low Earth orbit at 700-km altitude. A key mission objective is to demonstrate onboard, fully autonomous, robust, safe, and precise formation flying of spacecraft. This is accomplished by spaceborne global positioning system navigation, guidance, and control functionalities for the maintenance of the relative motion between the two spacecraft. An innovative estimation approach employs a common Kalman filter for the absolute states of Main and Target, which accounts for the interdependency of absolute and relative navigation without the need for an explicit relative state. As a result, the onboard navigation system provides absolute and relative orbit information in real time with a position accuracy of 2 and 0.1 m, respectively. The formation control achieves accuracies of a few tenths of meters with minimum usage of thrusters. The guidance and control concept is detailed with emphasis on a relative eccentricity and inclination vector separation strategy. The paper derives estimates of the expected relative orbit control performances based upon real-world simulations using typical global positioning system receiver and propulsion system characteristics.

Nomenclature

a	=	semi-major axis
$\boldsymbol{a}$	=	acceleration vector
B	=	ballistic coefficient
C_D	=	drag coefficient
c	=	velocity of light
d_D	=	along-track acceleration due to drag
dt	=	time difference of filter updates
$\boldsymbol{E}$	=	transformation matrix
e	=	eccentricity
$\boldsymbol{e}$	=	eccentricity vector
$\boldsymbol{e}_N, \boldsymbol{e}_R, \boldsymbol{e}_T$	=	unit vectors in normal, radial, and tangential directions
$\boldsymbol{G}$	=	measurement partials vector
g	=	modeled measurement
h	=	numerical integrator step size
I	=	ionospheric bias
i	=	inclination
$\boldsymbol{i}$	=	inclination vector
J_2	=	second-order zonal coefficient of the geopotential
$\boldsymbol{K}$	=	Kalman filter gain vector
l	=	longitude
M	=	mean anomaly
N	=	integer bias of carrier phase
$\boldsymbol{N}$	=	integer bias vector
n	=	mean motion
$\boldsymbol{P}$	=	covariance matrix
$\boldsymbol{Q}$	=	process noise covariance matrix
$R_{\oplus}$	=	Earth equatorial radius
$\boldsymbol{r}$	=	radius vector of the spacecraft
$\ddot{\boldsymbol{r}}$	=	acceleration of the spacecraft
t	=	time
u	=	mean argument of latitude
$\boldsymbol{v}$	=	velocity of the spacecraft
W	=	measurement weight
$\boldsymbol{x}$	=	Kalman filter state
z	=	measurement
γ	=	J_2 perturbation coefficient
Δ	=	difference operator
Δl	=	relative mean longitude
Δt	=	drift time interval
$\Delta\alpha$	=	attitude control error
$\Delta\rho$	=	relative navigation error
δe	=	relative eccentricity vector amplitude
δi	=	relative inclination vector amplitude
δt	=	clock offset
$\delta\Delta$	=	relative difference operator, $\Delta(\cdot) - \Delta(\cdot)$
ϵ	=	differential ballistic coefficient
η	=	propulsion system performance
θ	=	relative ascending node
λ	=	wavelength
μ	=	Earth's gravitational coefficient
ρ	=	pseudorange
σ	=	process noise
τ	=	time scale of process noise
$\boldsymbol{\Phi}$	=	transition matrix
ϕ	=	carrier phase
φ	=	relative perigee
Ω	=	right ascension of the ascending node
ω	=	argument of perigee
$\nabla\Delta$	=	double-difference operator

Subscripts

a	=	acceleration
clk	=	clock
D	=	drag
emp	=	empirical acceleration
G	=	gravity
GPS	=	global positioning system
i	=	Kalman filter step
M	=	Main spacecraft of PRISMA formation
M	=	moon
N	=	normal
R	=	radial
S	=	sun
SR	=	solar radiation
T	=	total
T	=	tangential

*Scientist, German Space Operations Center, Space Flight Technology, currently Chairholder, Space Systems Engineering, Faculty of Aerospace Engineering, Delft University of Technology, Kluyerweg 1, 2629 HS Delft, The Netherlands.

T	=	Target spacecraft of PRISMA formation
x	=	x component of the vector
y	=	y component of the vector
0	=	initial condition
+	=	after measurement update
−	=	before measurement update

Superscripts

C/A	=	coarse acquisition GPS code
$L1$	=	GPS first fundamental frequency
max	=	maximum value
N	=	nominal

Introduction

FORMATION flying of satellites is a research topic that has led to a variety of ambitious mission proposals in the past [1]. However, actual experience in formation flying is limited in terms of specific formation flying technologies and their applications. Apart from rendezvous scenarios in the framework of manned missions [2], formation flying in low Earth orbit (LEO) is mainly restricted to a few scientific applications and technology demonstrations.

The gravity recovery and climate experiment (GRACE) [3] is a close LEO formation, in orbit since 2002, that operates at an along-track separation of 220 ± 50 km at 450-km altitude. However, its large control window only requires infrequent orbit maneuvers to adjust the relative orbit, which is manually executed via ground commands. The formation flying demonstration of the Earth-observing mission EO-1/Landsat in 2001 was conducted at 700-km altitude, with an along-track separation of 450 ± 85 km [4]. Since 2006, the CloudSat and Calipso spacecraft fly in formation as part of the so-called A-train of satellites, with an along-track separation of 112 ± 19 km [5]. In all of these cases, the large control window allows sparse maneuvers that can conveniently be executed by ground control. On the contrary, the demonstration of the autonomous rendezvous technology (DART) mission in 2005 attempted to rendezvous completely autonomously with, and to perform a variety of maneuvers in close proximity to, the multiple-paths-beyond-line-of-sight communications (MUBLCOM) satellite. However, DART did not meet its main mission objectives and ultimately caused a collision with the MUBLCOM spacecraft [6]. The Experimental Satellite System-11 (XSS-11) was launched in 2005 and demonstrated several rendezvous and proximity operations with a launch vehicle upper stage. It will demonstrate an increasing level of autonomy as the project continues.

In the regime of scientific applications in LEO, formation flying is of major interest for interferometric synthetic aperture radar (SAR) applications [7]. Here, short to medium separations of spacecraft lead to close formations that require autonomous formation keeping. An example of an interferometric SAR formation flying mission is TSX/TDX [8] (TerraSAR-X/TanDEM-X), recently selected as a new Earth-observation mission within the German national space program. TSX/TDX will form a radar interferometer orbiting at 500-km altitude, with typical baselines of about 1 km, and will require daily orbit maneuvers implemented via either ground-in-the-loop control with a high level of automation [9] or complete onboard autonomy.

The motivation for this work is the development and demonstration of innovative global positioning system (GPS) guidance, navigation, and control (GNC) algorithms for fully autonomous, robust, and precise formation flying of future spacecraft. The demonstration will be accomplished within the PRISMA mission [10], which is a precursor mission for critical technologies for formation flying and in-orbit servicing. The PRISMA space segment will comprise the fully maneuverable Main minisatellite and the smaller Target satellite. A GPS-based navigation system on Main will process local GPS measurements and GPS measurements from Target, transmitted to Main by an intersatellite radio link, and will provide continuous and precise absolute and relative orbit information in real time. In addition, PRISMA will conduct the

spaceborne autonomous formation flying experiment (SAFE) with the objective to demonstrate a fully autonomous, robust, and precise formation flying of spacecraft. To this end, a fuel-optimized guidance and control algorithm will provide an accuracy of better than 25 m at typical spacecraft distances of 100 to 2000 m, which is representative of future interferometric SAR formation flying missions like TSX/TDX. SAFE will acquire and maintain robust and safe close formation flying configurations in complete autonomy over long time intervals (weeks).

In the past, onboard navigation systems for rendezvous and formation flying applied a mixture of absolute and relative navigation for the filter states and their dynamics [2,11,12]. A relative GPS navigation implementation [2] for the automated transfer vehicle (ATV) applies single-difference pseudoranges to estimate the relative states based on a quasi-circular absolute orbit model. In [11], only relative filter states are estimated from double-difference carrier phases, whereas the dynamics are based on the numerical integration of the absolute orbits. In [12], one filter is implemented for the absolute navigation based on pseudorange and Doppler measurements, whereas a second filter for relative navigation assumes a Keplerian motion to process single-difference carrier-phase data. In the present paper, a unique concept for absolute and relative navigation is presented that is based on a single common Kalman filter for the absolute states of the two spacecraft and on the modeling of their dynamics. This completely abandons the need for relative filter states and associated relative dynamics and allows one to fully exploit the interdependency of absolute and relative dynamics. The filter applies pseudorange data from the two spacecraft for the robust reconstruction of the absolute orbits, whereas a precise and implicit determination of the relative orbit is achieved based upon ambiguity resolution of double-difference carrier-phase measurements. The concept is robust in terms of the attitude of the spacecraft, because the relative orbit can still be determined from pseudoranges, should double-difference carrier phases of commonly viewed GPS satellites not be available. The relative state vector and its associated covariance matrix may easily be computed external to the filter without any further limitations and assumptions.

The guidance and control of satellite formations is typically described using the Cartesian comoving triad defined as part of the Hill–Clohessy–Wiltshire (HCW) equations [13,14]. These equations describe the motion of a spacecraft relative to a circular reference orbit under the assumptions that the spacecraft separations are small with respect to their geocentric distance and that the motion is purely Keplerian. Because the HCW equations neglect the significant perturbations of the second-order zonal coefficient J_2 caused by the Earth's oblateness, considerable effort was put into their extensions to incorporate these contributions [15,16]. In this paper, guidance and control of satellite formations is instead described in terms of relative orbital elements, which simplifies the formation flying design and gives immediate insight into the geometry of the formation [9]. In particular, it separates the relative eccentricity/inclination vectors through the proper configuration of the two spacecraft in radial and cross-track direction. This allows passively stable formation flying configurations and avoids collision hazard from along-track position uncertainties. Furthermore, short- and long-term and secular perturbations due to J_2 may easily be incorporated into the method. This technique has its roots in the colocation of geostationary satellites [17] and was successfully adopted for the first time in LEO to safely switch the satellites of the GRACE formation [18]. In this paper, the method is applied, for the first time, to a long-term simulation of autonomous formation control in the presence of realistic sensors and actuators.

This paper introduces the PRISMA mission [10], addressing its objectives, orbit characteristics, and spacecraft design; emphasis is given to a description of the selected GPS receiver and thruster characteristics. Furthermore, the concept for data handling and onboard software development is described, supplemented by a presentation of the architecture of the GPS-based onboard GNC software. The second part of the paper provides a description of the GPS-based GNC algorithms. Here, the measurement and dynamical

models are detailed and the applied filter concept is specified. The SAFE formation control design describes the relative motion of the participating satellites in terms of relative orbital elements. The model accounts for the second-order zonal coefficient J_2 and makes use of the theories of Brouwer [19] and Lyddane [20] for the computation of mean relative orbital elements. A deterministic impulsive orbit control strategy is shown to be a straightforward application of the Gauss variational equations [21] in combination with the adopted relative motion model. Impulsive maneuvers are easily planned to counteract non-Keplerian orbital perturbations to maintain and/or reconfigure the formation. Finally, the paper presents simulation results of the relative orbit guidance and control laws in the presence of real-world dynamics, including the modeling of sensors and actuators.

PRISMA Mission

Mission Description

The mission objectives of PRISMA may be divided into the validation of sensor and actuator technologies related to formation flying and the demonstration of experiments for formation flying and rendezvous. Key sensor and actuator components [10] comprise a GPS receiver system, two vision-based sensors, two formation flying radio frequency sensors, and a high-performance green propellant system. These will support and enable the demonstration of autonomous spacecraft formation flying, homing, and rendezvous scenarios, as well as close-range proximity operations.

The mission schedule foresees a launch of the two spacecraft in the second half of 2008. Both Main and Target will be injected by a Dnepr launcher into a sun-synchronous orbit at 700-km altitude and 98.2-deg inclination. A dusk–dawn orbit with a 6 or 18 h nominal local time at the ascending node (LTAN) is targeted. Maximum eclipse times of 23 min may occur for injections within ±1 h off the nominal LTAN, depending on the sun's declination.

Following a separation from the launcher, the two spacecraft will stay in a clamped configuration for initial system checkout and preliminary verification. Once the spacecraft are separated from each other, various experiment sets for formation flying and in-orbit servicing will be conducted within a minimum targeted mission lifetime of eight months.

Spacecraft operations will be performed remotely from Solna, near Stockholm, making use of the European Space and Sounding Rocket Range (Esrange) ground station in northern Sweden. The S-band ground–space link to Main supports commanding with a bit rate of 4 kbps and telemetry with up to 1 Mbps. In contrast, communication with the Target spacecraft is only provided through Main acting as a relay and making use of a Main–Target intersatellite link (ISL) in the ultrahigh-frequency (UHF) band with a data rate of 19.2 kbps.

Space Segment

The Main spacecraft has a wet mass of 150 kg and a size of $80 \times 83 \times 130$ cm in launch configuration. In contrast to the highly maneuverable Main spacecraft, Target is a passive and much simpler spacecraft, with a mass of 40 kg at a size of $80 \times 80 \times 31$ cm (Fig. 1). Electrical power for the operation of the Main spacecraft bus and payload is provided by two deployable solar panels delivering a maximum of 300 W, whereas Target relies on one body-mounted solar panel providing a maximum of 90 W.

GNC Sensor and Actuator Overview

The Main spacecraft implements a three-axis, reaction-wheel-based attitude control and three-axis delta-V capability. To this end, the Main GNC sensors comprise two three-axis magnetometers, one pyramid sun acquisition sensors, five sun-presence sensors, five single-axis angular-rate sensors, five single-axis accelerometers, two star-tracker camera heads for inertial pointing, and two GPS receivers. As actuators, three magnetic torque rods, four reaction wheels, and six thrusters are employed.

The Target spacecraft applies a coarse three-axis attitude control based on magnetometers, sun sensors, and GPS receivers (similar to Main), with three magnetic torque rods as actuators. The nominal attitude profile for Target will be sun or zenith pointing.

GPS Receiver

Phoenix is a miniature GPS receiver for high-dynamics and space applications. The Phoenix receivers to be flown on PRISMA are 12-channel single-frequency GPS receivers based on a commercial off-the-shelf hardware platform and qualified by DLR, German Aerospace Center for use in LEO [22]. Phoenix offers single-frequency coarse/acquisition (C/A) code and carrier tracking and can be aided with a priori trajectory information to safely acquire GPS signals even at high altitudes and velocities. Upon tracking, Phoenix outputs a one-pulse-per-second (1PPS) signal and aligns the message time tags to integer GPS seconds, which facilitates differential measurement processing.

The receiver is built around the GP4020 baseband processor by Zarlink Semiconductor Inc., which combines the correlator, a microcontroller core with a 32-bit ARM7TDMI microprocessor, and several peripheral functions in a single package. Phoenix provides a code-tracking accuracy of better than 0.5 m and a carrier-phase
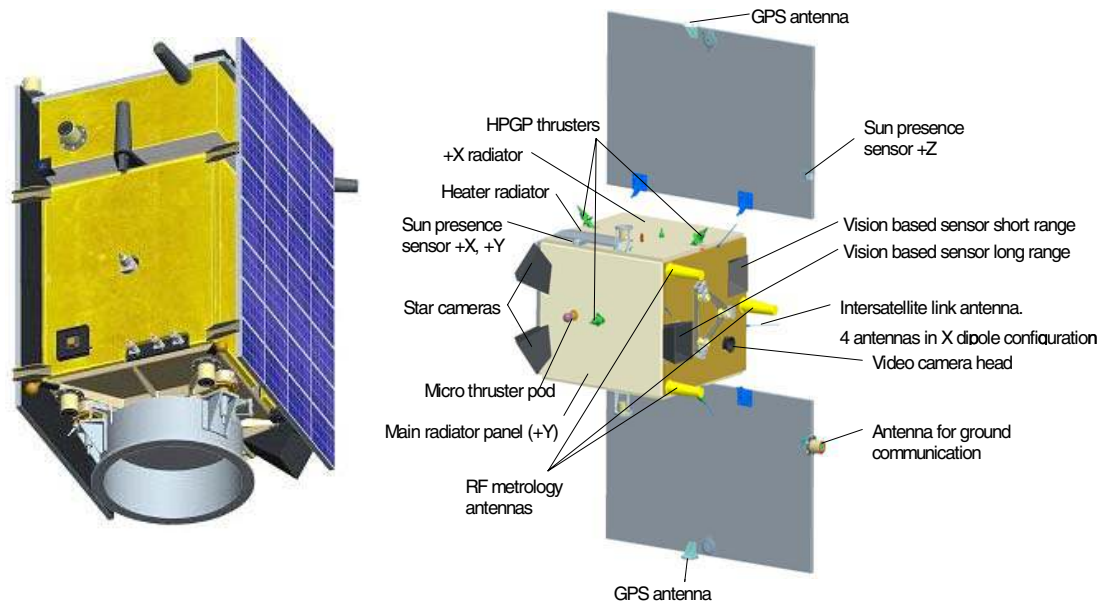

Fig. 1   Launch configuration (left) of the Main (bottom) and Target (top) spacecraft; separated Main spacecraft (right).
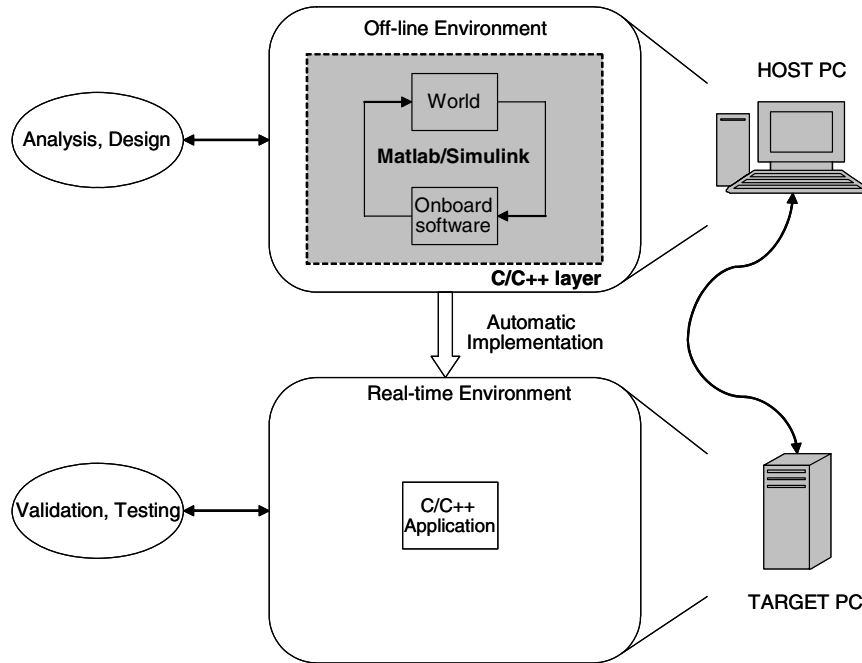
Fig. 2 Flight software design for PRISMA.

accuracy of better than 1 mm at 45 dBHz. With a receiver board mass of 20 g and a power consumption of 0.85 W at beginning of life, the receiver is particularly suited for small satellite missions.

Thruster System

The Main spacecraft will accommodate a hydrazine-based thruster system that provides delta-V for relative navigation with respect to Target. The system will provide thrust in all directions, using six 1-N thrusters that are capable of providing impulse bits ranging from 0.1 Ns up to continuous burns of 30 s, with a maximum pulse rate of 1 Hz. Minimum impulse bits translate to single velocity increments of 0.7 mm/s, which can be applied for formation control. A total of 11 kg of propellant provides a total delta-V of 115 m/s in an accumulated firing time of at least 5 h [23].

Data Handling and Onboard Software

The core of the data handling system (DHS) on Main is the spacecraft controller based on a LEON3 microprocessor. LEON3 implements a 32-bit processor compliant with the SPARC V8 architecture, which is particularly suited for embedded applications [24]. In contrast to its predecessor LEON2, LEON3 recognizes bit flips and is fault-tolerant. Its implementation through a field-programmable gate array (FPGA) by Atmel Corporation provides a performance of about 20 MIPS and accommodates one floating point unit (FPU). Communication between platform units and the spacecraft controller is implemented via a controller area network (CAN) bus.

The onboard software (OBS) architecture consists of a layered structure with a basic software (BSW) level and an application software (ASW) level communicating with each other through dedicated message queues. Although the BSW includes basic applications, device drivers, and I/O utilities, the ASW encapsulates all top-level applications such as spacecraft control, telecommand, and telemetry. A model-based design method is used for the ASW layer, which is grouped into functionally encapsulated application components. The onboard software is implemented in Matlab, Simulink, and C/C++ functions (cf. Fig. 2), which are then autocoded with Real-Time Workshop (RTW) and executed under the operating system real-time executive for multiprocessor systems (RTEMS) on the LEON3.

The flight software development will follow two phases: the design phase and the integration, test, and validation phase. The aim

of the first phase is to develop the onboard GNC functionalities (cf. the onboard software in Fig. 2) and to model the external environment in terms of natural forces, sensors, and actuators (cf. the world in Fig. 2). The prototyping of the software and the related analysis and simulations are performed in this phase using a standard host computer (cf. the host PC in Fig. 2). The test and validation phase applies RTW and initiates the application program on the real-time hardware (cf. the target PC in Fig. 2).

A schematic representation of the software architecture for autonomous formation flying is depicted in Fig. 3. For an efficient implementation, the architecture comprises two cores: the ORB core, which is executed every 30 s and the GNC core, executed once per second to clearly separate the computationally intensive GPS-based orbit determination from functions with low computational burden. The GPS interface handles GPS raw data formats and ephemerides and performs data sampling and coarse editing before the GPS-based orbit determination. The GPS orbit prediction function evaluates the orbit, provided by the orbit determination function, at a 1-Hz rate and accounts for orbit maneuvers, which might have been executed by the Main spacecraft in the past 30 s. It also outputs the Main and Target orbit states, which are used by other onboard GNC functions and by the autonomous formation control function implementing the specific guidance and control algorithms described in the next section.

GPS-Based Navigation, Guidance, and Control

Navigation

The GPS-based navigation system onboard the Main will process local raw GPS measurements and code and carrier-phase measurements transmitted from the Target by an intersatellite radio link. The Main and Target attitude data are applied to correct for the GPS receiver antenna offset with respect to the spacecraft center of mass. Orbit maneuver data of the Main spacecraft is accounted for in the orbit prediction. The navigation system will provide continuous absolute position and velocity data of the Main and Target at a 1-Hz data rate for GNC functions and the PRISMA payload.

Measurement Model

As a baseline, orbit determination of the Main and Target is based on C/A pseudoranges $\rho^{C/A}$, which are modeled as [25]

$$\rho^{C/A} = \rho + c(\delta t - \delta t_{\text{GPS}}) + I \qquad (1)$$
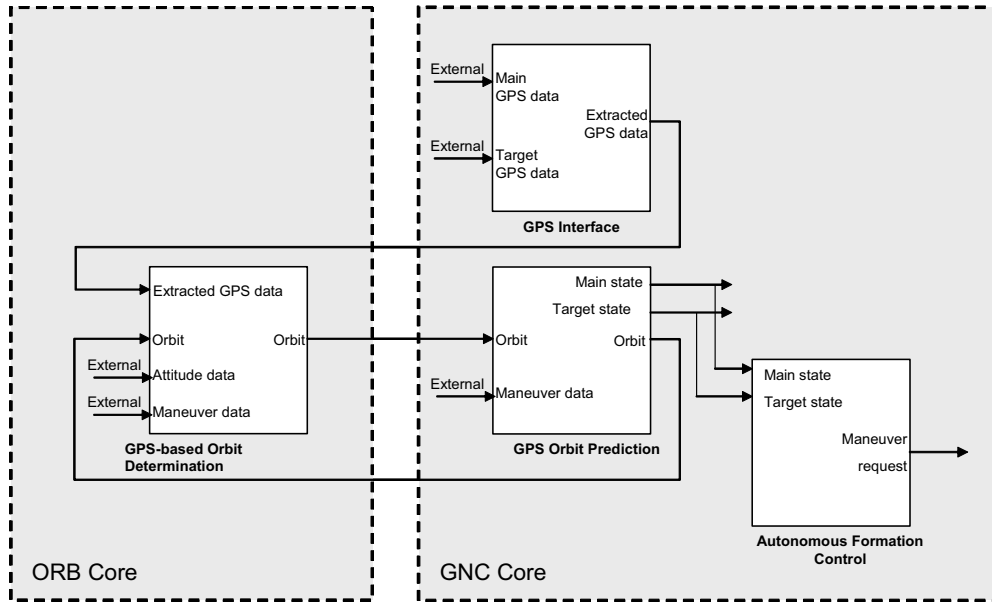
Fig. 3   Schematic software architecture for PRISMA GPS-based autonomous formation flying.

Alternatively, a combination of pseudorange and L1 carrier-phase measurements ρ^{L1} could be applied, which is denoted as a group and phase ionospheric calibration (GRAPHIC) data type [26]. GRAPHIC data are free from ionospheric errors, because the ionospheric group delay in pseudorange measurements is equal in size but opposite in sign to the ionospheric phase change in carrier-phase measurements. Using GRAPHIC data for PRISMA would require a total of 24 additional estimation parameters (i.e., the GRAPHIC biases from the 12-channel receivers on Main and Target), which would significantly increase the filter complexity. A pure pseudorange-based orbit determination approach achieves, in a reduced-dynamic filter, position accuracies of up to 1 m [27].

For relative navigation, a double-difference processing of carrier-phase measurements with ϕ at λ fully exploits the accuracy potential of this data type. The measurement equation is given as

$$\nabla\Delta(\lambda\phi)_{MT}^{ij} = \nabla\Delta(\rho)_{MT}^{ij} + \nabla\Delta(\lambda N)_{MT}^{ij} - \nabla\Delta(I)_{MT}^{ij} \qquad (2)$$

where $\nabla\Delta$ is related to GPS satellites i and j and the receivers on Main and Target. Although differencing across receivers reduces broadcast ephemeris and ionospheric errors, the differencing across GPS satellites eliminates the user clock error and the initial fractional carrier phase. Still, the measurement equation requires the solution of the integer bias N and the treatment of the differential ionospheric error $\nabla\Delta(I)_{MT}^{ij}$.

Trajectory Model

Although a purely dynamic force model does not provide the necessary accuracy to adequately fit precise GPS measurements over extended data arcs, a kinematic approach would neglect orbit knowledge from the equations of motion to improve the orbit determination accuracy. Thus, a reduced-dynamic approach was adopted for orbit determination. To this end, the acceleration of the spacecraft is modeled according to [28]

$$\ddot{\boldsymbol{r}} = \ddot{\boldsymbol{r}}_G + \ddot{\boldsymbol{r}}_S + \ddot{\boldsymbol{r}}_M + \ddot{\boldsymbol{r}}_D + \ddot{\boldsymbol{r}}_{SR} + \boldsymbol{E}\boldsymbol{a}_{\text{emp}} \qquad (3)$$

where $\ddot{\boldsymbol{r}}_G, \ddot{\boldsymbol{r}}_S, \ddot{\boldsymbol{r}}_M, \ddot{\boldsymbol{r}}_D$, and $\ddot{\boldsymbol{r}}_{SR}$ account for the complex gravity field of the Earth (complete to order and degree 20 in the spherical harmonic expansion of the field), third-body accelerations from the sun and the moon, and atmospheric drag and solar radiation pressure. The deficiency in the assumed force model is accounted for by an empirical acceleration vector $\boldsymbol{a}_{\text{emp}}$ (with components in the radial,

along-track, and cross-track directions), which is transformed by the matrix $\boldsymbol{E}$ to the reference system in which the numerical integration is performed.

The navigation algorithm employs an advanced numerical integration scheme, which extends the common Runge–Kutta fourth-order algorithm (RK4) by Richardson extrapolation and a fifth-order Hermite interpolation [29]. The algorithm comprises two elementary RK4 step sizes of length h and can be shown to be effectively of the fifth order, with six function calls per h. The Hermite interpolation of the spacecraft position allows for an efficient provision of dense position output at a rate of 1 Hz, whereas typical step sizes of the numerical integration scheme are 30 to 60 s.

The transition and sensitivity matrices are derived from a numerical integration of the variational equations. To this end, the partial derivatives are computed based on a numerical difference approximation. Aside from the increased accuracy compared with an analytical computation of the transition matrix, this approach is general and flexible enough to estimate additional force model parameters. The computational load for the numerical integration of the variational equations is kept minimum by accounting only for Earth gravity field coefficients up to the second-order zonal term.

Filter Model

An extended Kalman filter will be employed for the onboard orbit determination. Earlier approaches for GPS-based onboard orbit determination of a satellite formation typically separated the problem into the reconstruction of absolute and relative orbits [11,12]. In [11], the state vector for the absolute orbit of a spacecraft was estimated from GRAPHIC data and comprised the absolute position (3), velocity (3), empirical accelerations (3), receiver clock offset (1), and carrier-phase biases (12). The state vector for the relative orbit determination was derived from double-difference carrier-phase measurements and comprised the relative position (3), relative velocity (3), ionospheric delay (1), and integer carrier-phase ambiguities (12). Although this concept requires $22 + 19 = 41$ estimation parameters in total and is efficient in terms of its computational load, its inherent drawback is the separation of the absolute and the relative filter, which does not exploit the interdependency of absolute and relative dynamics. Furthermore, it exhibits a lack of robustness, because the state of the second satellite is only reconstructed from the double-difference carrier-phase measurements that require common visibility of GPS satellites. This severely constrains the attitude modes of the spacecraft in the formation and may not be acceptable for general formation flying missions, in particular, not for PRISMA.

An innovative filter concept was developed for PRISMA that employs a common Kalman filter for the absolute states of Main and Target without the need for an explicit relative state. It applies pseudorange data from Main and Target to estimate their absolute orbits and double-difference carrier-phase measurements to implicitly determine their relative orbit with high precision. The associated 35-dimensional state vector x is given by

$$x = (r_M, v_M, a_{empM}, C_{D_M}, \delta t_M, r_T, v_T, a_{empT}, C_{D_T}, \delta t_T, I, N) \quad (4)$$

which comprises the absolute position r (3), absolute velocity v (3), empirical acceleration a_{emp} (3), drag coefficient C_D (1), receiver clock offset δt (1), ionospheric zenith delay I (1), and the vector of integer carrier-phase ambiguities N (12). This concept provides a symmetric filter design in terms of Main and Target, which fully exploits the dynamic information for absolute and relative motion. Although the accuracy of the absolute states is only slightly improved by the addition of double-difference carrier phases, the accuracy of the relative state, which is easily derived by the difference of the absolute states, takes maximum advantage from the highly precise double-difference carrier phases, because integer ambiguities are solved. Furthermore, the filter design assures robustness in case Main and Target do not have common GPS satellites in view. Finally, the handling of orbit maneuvers is greatly simplified, because the concept of absolute and relative navigation is abandoned.

Because the Phoenix GPS receiver provides its measurements synchronized to integer GPS seconds, the filter implementation is also simplified, because a common measurement epoch t_i can be chosen for which the Main and Target pseudorange and carrier phases are available. The *time update* of the filter at step i comprises the interpolation of the orbit polynomials at time t_i to assemble the predicted state vector x_i^- and to compute the associated covariance matrix P_i^- based on the transition matrix Φ_i and the process noise matrix [28] Q_i

$$x_i^- = x\left[t_i; x(t_{i-1}) = x_{i-1}^+\right], \qquad P_i^- = \Phi_i P_{i-1}^+ \Phi_i^T + Q_i \quad (5)$$

The *measurement update* phase is then given by

$$K_i = P_i^- G_i^T (W_i^{-1} + G_i P_i^- G_i^T)^{-1}$$
$$x_i^+ = x_i^- + K_i(z_i - g_i), \qquad P_i^+ = (1 - K_i G_i) P_i^- \quad (6)$$

It is noted that scalar measurement updates are applied to avoid time-consuming matrix-vector operations.

A process noise matrix is employed to cope with residual modeling deficiencies and to keep the Kalman filter receptive to new measurements. To increasingly decorrelate estimates of the empirical accelerations and receiver clock offsets with the time difference of subsequent filter updates dt, their corresponding components of the process noise matrix Q_a and Q_{clk} are derived from a Gauss–Markov model for the empirical accelerations and a white noise model for the clock state according to

$$Q_a = \sigma_a^2[1 - \exp(-2dt/\tau_a)], \qquad Q_{clk} = \sigma_{clk}^2 dt/\tau_{clk} \quad (7)$$

with the respective process noise amplitudes σ_a and σ_{clk} and their characteristic process noise time scales τ_a and τ_{clk}.

Guidance and Control

The GPS-based navigation system on PRISMA will be complemented by guidance and control algorithms to conduct an experiment demonstrating a fully autonomous, robust, and precise formation flying of spacecraft. To this end, fuel-optimized formation flying at typical distances of 100 to 2000 m is foreseen, which is representative of future satellite formation flying missions [30] that will implement interferometric SAR applications.

Linear Relative Motion Model

The relative motion of the Main spacecraft is described in Hill's [13] coordinate frame, centered at the position of the Target spacecraft. Its orientation is given by the triad of unit vectors $\{e_R, e_T, e_N\}$, where e_R is aligned with the radial direction (positive outwards) and e_N is parallel to the orbit momentum vector. The vector e_T then completes the right-hand coordinates system. The relative position and velocity vectors of Main with respect to Target Δr and Δv are expressed in the Hill frame as

$$\Delta r = r_M - r = \Delta r_R e_R + \Delta r_T e_T + \Delta r_N e_N$$
$$\Delta v = v_M - v = \Delta v_R e_R + \Delta v_T e_T + \Delta v_N e_N \quad (8)$$

where r and v and r_M and v_M are the inertial position and velocity vectors of Target and Main, respectively. In the following, the subscript M denotes the Main parameters, whereas no subscript is used for Target.

In parallel with a Hill [13] Cartesian coordinates representation of the relative motion, a description in terms of relative orbital elements can be adopted that simplifies the formation flying design and gives immediate insight into the geometry of the constellation [9]. The relative orbital elements parameterization is based on the relative semi-major axis Δa, the relative mean argument of latitude Δu, the relative eccentricity vector $\Delta e = (\Delta e_x, \Delta e_y)^T$, and the relative inclination vector $\Delta i = (\Delta i_x, \Delta i_y)^T$. The six relative orbital elements are defined as the difference of the orbital elements of Main and Target, according to

$$\Delta a = a_M - a, \qquad \Delta e_x = e_M \cos \omega_M - e \cos \omega$$
$$\Delta i_x = i_M - i, \qquad \Delta u = u_M - u \quad (9)$$
$$\Delta e_y = e_M \sin \omega_M - e \sin \omega, \qquad \Delta i_y = (\Omega_M - \Omega) \sin i$$

The relative eccentricity vector characterizes the periodic in-plane relative motion by combining the Keplerian elements e and ω. The relative inclination vector characterizes the periodic out-of-plane relative motion by combining the Keplerian elements i and Ω. The mean argument of latitude is the sum of the argument of perigee and the mean anomaly (i.e., $u = \omega + M$).

Depending on the specific application, either a Cartesian or a polar representation of the relative e/i vectors is preferable with the notation

$$\Delta e = \delta e \begin{pmatrix} \cos \varphi \\ \sin \varphi \end{pmatrix}, \qquad \Delta i = \delta i \begin{pmatrix} \sin \theta \\ \cos \theta \end{pmatrix} \quad (10)$$

The amplitudes of the relative e/i vectors are δe and δi, and the phases of the relative e/i vectors are φ and θ.

The description of the relative motion in terms of the Cartesian coordinates vector Δr defined in Eq. (8) can be derived from the Clohessy–Wiltshire (CW) equations [14]. The general closed-form solution of the CW equations using the mean argument of latitude as an independent variable [31] is

$$\begin{cases} \Delta r_R/a = \Delta a/a - \delta e \cos(u - \varphi) \\ \Delta r_T/a = \Delta l - (3/2)(\Delta a/a)(u - u_0) + 2\delta e \sin(u - \varphi) \\ \Delta r_N/a = \delta i \sin(u - \theta) \end{cases}$$

$$(11)$$

where $u_0 = u(t_0)$ is the mean argument of latitude at the initial time t_0, and $\Delta l = \Delta u + \Delta \Omega \cos i$ is the difference of the mean orbital longitudes of both spacecraft. Equation (11) is a convenient basis for the analyses of rendezvous and formation flying. For the PRISMA formation, we are only interested in close relative orbits of the Main spacecraft centered at the Target spacecraft, which is described by $\Delta a = 0$ and $\Delta u = -\Delta \Omega \cos i$. The resulting relative motion is completely determined by the amplitude and phase of the relative e/i vectors, as depicted in Fig. 4. The in-plane relative motion depends
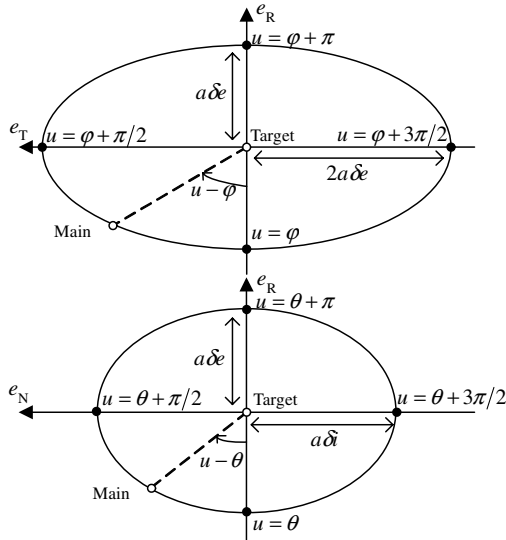
Fig. 4 Relative motion of Main with respect to Target, with e/i vector separation; in-plane (top) and out-of-plane (bottom) motion in the Hill [13] frame.

on the relative eccentricity vector, whereas the out-of-plane motion depends on both the eccentricity and inclination vectors.

Collision avoidance between the PRISMA spacecraft can easily be handled by means of the e/i vector separation concept. For (anti-) parallel e/i vectors (i.e., $\varphi = \theta$), the minimum distance between Main and Target is given by $\min(a\delta e, a\delta i)$. The projection of the relative trajectory onto the orbital plane is an ellipse of the semi-major axis $2a\delta e$ in the along-track direction and of the semi-minor axis $a\delta e$ in the radial direction. The projection onto the plane perpendicular to the flight direction is an ellipse of the semi-major axis $\max(a\delta e, a\delta i)$ and the semi-minor axis $\min(a\delta e, a\delta i)$, in the radial and cross-track directions. This describes a collision-free configuration in which radial and cross-track separations never vanish at the same time (i.e., at the same mean argument of latitude). Perpendicular e/i vectors denote, instead, a dangerous configuration, especially in the case of large uncertainties in along-track separation.

The relative motion of formation flying spacecraft in the presence of an oblate Earth may be derived from the inclusion of perturbations of J_2 into the linear relative motion model. Following Brouwer [19] and Lyddane [20], the J_2 short-period variations of the orbital elements only depend on the mean argument of latitude. Consequently, these perturbations can be neglected when computing the relative orbital elements for close formation flying satellites. The remaining J_2 effects are the secular variations of the argument of perigee, the right ascension of the ascending node, and the mean anomaly

$$\frac{d\omega}{du} = \frac{3}{2}\gamma(5\cos^2 i - 1), \qquad \frac{d\Omega}{du} = -3\gamma\cos i$$
$$\frac{dM}{du} = 1 + \frac{3}{2}\gamma\sqrt{1-e^2}(3\cos^2 i - 1) \tag{12}$$

with

$$\gamma = \frac{J_2}{2}\left(\frac{R_\oplus}{a}\right)^2 \frac{1}{(1-e^2)^2} \tag{13}$$

Upon substituting Eq. (12) into the derivatives of the relative orbital elements defined by Eq. (9) and integrating over an arbitrary time interval, we obtain, to first order in the relative orbital elements, the secular growth of the relative orbital elements. The resulting linear relative motion model is

$$\begin{cases} \Delta r_R/a = \Delta a/a - \delta e \cos[\varphi_0 + \varphi'(u-u_0)] \\ \Delta r_T/a = \left[\Delta l_0 - \frac{21}{2}\gamma\Delta i_x(u-u_0)\sin 2i\right] \\ \qquad\qquad - \frac{3}{2}\frac{\Delta a}{a}(u-u_0) + 2\delta e \sin[\varphi_0 + \varphi'(u-u_0)] \\ \Delta r_N/a = [-\Delta i_{y0} - 3\gamma\Delta i_x(u-u_0)\sin^2 i]\cos u + \Delta i_x \sin u \end{cases}$$
$$\tag{14}$$

where the subscript 0 was introduced for the initial conditions of time-dependent elements and

$$\varphi' = \frac{d\varphi}{du} = \frac{3}{2}\gamma(5\cos^2 i - 1) \tag{15}$$

is the derivative of the relative perigee. Only the relative semi-major axis Δa and the x component of the relative inclination vector Δi_x are not affected by the J_2 perturbations. The other relative orbital elements experience a secular trend that is directly proportional to the elapsed time (i.e., $u - u_0$). In particular, the relative eccentricity vector evolves along a circle of radius δe, being centered at the origin of the e vector plane and traversed at an angular velocity given by Eq. (15). The relative inclination vector is likewise affected by J_2 perturbations causing a linear drift of the Δi_y component proportional to inclination difference Δi_x. Finally, the relative mean longitude between the spacecraft exhibits a secular trend that is proportional to the inclination difference.

Impulsive Relative Orbit Control

The maintenance of the PRISMA formation requires the performance of maneuvers to counteract gravitational perturbations due mainly to J_2 and differential drag effects. Among the various control methods, an impulsive feedback control was selected that minimizes the number of maneuvers, as shown in previous studies [32], while maximizing the time for data collection.

The equations for the impulsive relative orbit control of spacecraft in near-circular nonequatorial orbits are obtained through the integration of the Gauss variational equations over the impulsive maneuver, as

$$\begin{cases} \delta\Delta a/a = +2\cdot\Delta v_T \\ \delta\Delta u = -2\cdot\Delta v_R - \frac{\sin u}{\tan i}\cdot\Delta v_N \\ \delta\Delta e_x = +\sin u\cdot\Delta v_R + 2\cos u\cdot\Delta v_T \\ \delta\Delta e_y = -\cos u\cdot\Delta v_R + 2\sin u\cdot\Delta v_T \\ \delta\Delta i_x = +\cos u\cdot\Delta v_N \\ \delta\Delta i_y = +\sin u\cdot\Delta v_N \end{cases} \tag{16}$$

where $\Delta v = \mu/a^2(\Delta v_R, \Delta v_T, \Delta v_N)^T$ denotes the velocity increments expressed in the Hill [13] frame, and $\delta\Delta(\cdot)$ is the operator representing the difference between the relative orbital elements of Main after and before the maneuver impulse.

The relative orbit control system must be able to plan and execute correction maneuvers in accordance with predefined nominal relative orbital elements $\Delta a^N, \Delta u^N, \Delta e^N$, and Δi^N. In general, the actual orbital differences $\Delta a, \Delta u, \Delta e$, and Δi are confined within symmetric control windows centered around the nominal values. In this case, the control error of each of the relative orbital elements $\|\delta\Delta(\cdot)\| = \|\Delta(\cdot) - \Delta(\cdot)^N\|$ must be confined within $\pm\delta\Delta(\cdot)^{\max}$, with a total control window of $2\delta\Delta(\cdot)^{\max}$ for each relative orbital element. In the sequel, the relative orbital elements are understood as mean relative elements in which the J2 short-period perturbations have been removed using the algorithms of Brouwer [19] and Lyddane [20].

The relative inclination vector is optimally corrected by a single cross-track impulse, given by

$$\Delta v_N = 2\|\delta\Delta i\|, \qquad u = \arctan\frac{\delta\Delta i_y}{\delta\Delta i_x} \tag{17}$$

where $\delta\Delta i = (\Delta i^N - \Delta i)$ is the tracking error of the relative inclination vector computed at the time of the impulse. Applying this

maneuver corrects the relative inclination vector, but affects the relative mean argument of latitude. The undesired cross coupling is maximum if the thrust is performed at the extreme southern/northern latitudes, minimum if performed at the equator crossings, and ultimately depends on the magnitude of the desired correction of the relative inclination vector (i.e., on the out-of-plane maneuver cycle).

The correction of the remaining relative orbital elements is performed with two along-track impulsive maneuvers with amplitudes Δv_T^1 and Δv_T^2, located at the argument of latitudes u^1 and u^2:

$$\Delta v_T^1 = \tfrac{1}{4}(2\|\delta\Delta e\| + \delta\Delta a/a), \qquad u^1 = \arctan\frac{\delta\Delta e_y}{\delta\Delta e_x} \quad (18)$$

$$\Delta v_T^2 = -\tfrac{1}{4}(2\|\delta\Delta e\| - \delta\Delta a/a), \qquad u^2 = u^1 + \pi$$

where $\delta\Delta e = (\Delta e^N - \Delta e)$ is the tracking error of the relative eccentricity vector, and $\delta\Delta a = \Delta a^N - \Delta a$ is the tracking error of the relative semi-major axis. Both $\delta\Delta e$ and $\delta\Delta a$ have to be computed before the first impulse (i.e., Δv_T^1) for a real-time implementation of the feedback control law.

The correction of the relative mean argument of latitude is obtained through Eq. (18) via a proper choice of the nominal relative semi-major axis Δa^N. In contrast to the other relative orbital elements, Δu cannot be changed simultaneously by a tangential maneuver. Instead, a desired mean longitude drift is introduced in the time between the maneuver pairs, so that the mean along-track separation of the spacecraft can be confined within the desired longitude window.

The computation of the nominal relative semi-major axis is crucial for the firing scheme, because Δa^N depends on the a priori knowledge of the mean relative longitude drift experienced by the formation flying spacecraft. The size of Δa^N in Eq. (18) can be derived from an analytical estimation of the secular variation of the mean relative argument of latitude Δu_T, which includes the perturbations from J_2, Δu_{J2}, and from differential drag, Δu_D. Using Eq. (14), we obtain

$$\Delta u_T = \Delta u_{J_2} + \Delta u_D = -12\gamma\sin(2i)\Delta i_x n\Delta t + \frac{\varepsilon|d_D|}{2a}\Delta t^2 \quad (19)$$

where $\epsilon = (B_M - B)/B$ is the relative difference between the ballistic coefficients of Main (B_M) and Target (B). We can now close the deterministic feedback control law evaluating the nominal relative semi-major axis for the next in-plane maneuver cycle, as

$$\Delta a^N = -\frac{2}{3}\frac{a^2}{v}\frac{(\Delta u^N + 2\delta\Delta u^{\max} - \Delta u_T)}{\Delta t} \quad (20)$$

where $\delta\Delta u^{\max}$ has to be selected such as to guarantee a mean relative longitude window centered on the nominal relative mean argument of latitude Δu^N, according to

$$\delta\Delta u^{\max} = |-\tfrac{3}{2}\pi\Delta v_T^1| \quad (21)$$

The impulsive control law given by Eqs. (17–21) is simple, requires a low computational burden, and is thus ideally suited for an onboard autonomous implementation. The disadvantage of the presented algorithm is the necessity to analytically determine the drift of the relative mean argument latitude. Applied to PRISMA, the method relies on the knowledge of the differential drag acceleration between the Main and Target spacecraft.

Concept Validation
Navigation

The presented concept for GPS-based absolute and relative navigation was validated within a hardware-in-the-loop (HIL) demonstration. To this end, a signal simulator generated GPS signals for a LEO space scenario, which were received by Orion's GPS receivers (the predecessor of Phoenix, with comparable performance). The raw GPS measurements were transferred through radio modems to a central navigation computer for subsequent filtering

[11]. For the relative motion of two spacecraft, an ellipse with 4-km maximum along-track separation and 2-km radial separation was adopted that is representative for the PRISMA mission.

Results from HIL demonstrations for relative navigation exhibit a relative navigation accuracy (3-D RSS) after convergence is about 1.5 mm in relative position and 5 μm/s in relative velocity. At larger separations of 10–50 km, this accuracy degrades to 10 cm maximum, due to differential broadcast ephemeris and ionospheric errors. Although this accuracy may not be achievable for PRISMA due to multipath effects, coverage problems, and heavy maneuver activity, real-time relative navigation accuracies of better than 0.1 m (3D RSS) are expected. For absolute navigation, a position accuracy of better than 2 m will be achieved that is largely governed by GPS broadcast ephemeris errors.

In addition to the onboard navigation, an onground ex postfacto trajectory reconstruction will provide precise absolute and relative position and velocity data for verification and calibration purposes. In this context, ionosphere-free code-carrier combinations allow the estimation of absolute positions of the two PRISMA spacecraft with a 3-D accuracy of better than 0.5 m [26], and, subject to multipath avoidance and good common satellite visibility, relative positions with centimeter accuracy. The improvements over an onboard processing stem from the use of precise GPS clock and ephemeris data, distributed by the International GNSS Service (IGS), and from the use of more elaborate data editing and ambiguity resolution algorithms.

Guidance and Control

Even if $\varphi = \theta = \pi/2$ represents a constellation geometry with minimum collision risk, it does not always satisfy the science requirements, especially with SAR interferometric missions such as, for example, TanDEM-X [9]. To preserve the generality of the problem, the following representative formation flying configuration was selected:

$$a\delta e^N = 500 \text{ m}, \qquad \varphi^N = 80 \text{ deg}$$
$$a\delta i^N = 300 \text{ m}, \qquad \theta^N = 50 \text{ deg} \quad (22)$$

where $a = 7078.137$ km. The relative inclination vector has a nonzero x component, resulting in an inclination difference between the spacecraft orbits of $\Delta i_x = 1.56 \times 10^{-3}$ deg. Furthermore, selecting

$$\Delta a^N = 0, \qquad a\Delta u^N = -a\Delta i_y/\tan i = 33.1 \text{ m} \quad (23)$$

where $i = 98.2$ deg provides closed relative trajectories of Main centered around Target. An appropriate choice for the control windows is given by

$$a\delta\Delta i^{\max} = 5 \text{ m}, \qquad a\delta\Delta e^{\max} = 7 \text{ m}, \qquad a\delta\Delta u^{\max} = 20 \text{ m} \quad (24)$$

The objective of the following concept validation is to demonstrate the feasibility of the proposed orbit guidance and control concept and estimate the performance of the impulsive feedback control law. The guidance function comprises the computation of the difference of the actual and the nominal mean relative elements and the evaluation of deadband violations based on the defined control windows. The control function derives the maneuver times and sizes to shift the relative eccentricity/inclination vectors to the opposite side of the control window.

The described nominal formation configuration was simulated over a three-week time interval. To this end, a realistic dynamic model was applied in the numerical integration of the spacecraft motion. It comprises the Earth gravity model GGM01S up to order and degree 20, the lunisolar third-body gravitational perturbation, the lunisolar solid Earth tides, the atmospheric drag, and the solar radiation pressure. All models are supplemented by associated Earth rotation parameters and solar-geomagnetic data. Instead of using a dedicated orbit determination process, the GPS-based relative navigation filter was emulated by the nominal trajectories and
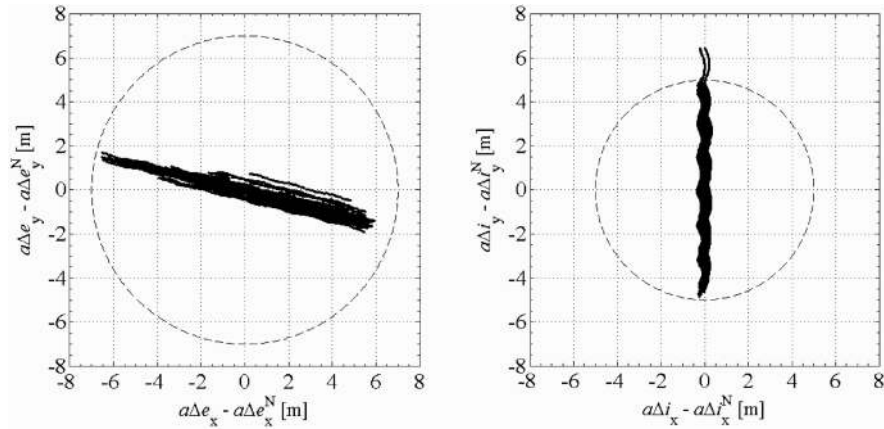
Fig. 5 Mean relative eccentricity vector (left) and mean relative inclination vector (right) errors over 21 days, based upon real sensors and actuators.
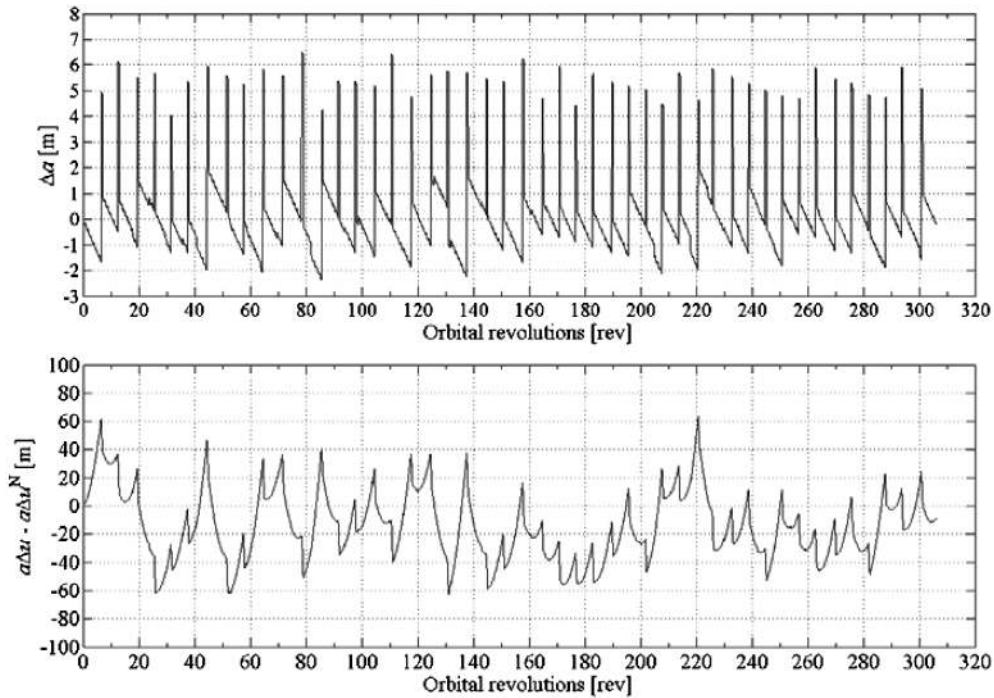

Fig. 6 Relative semi-major axis (top) and mean argument of latitude (bottom) with real sensors and actuators.

specific relative navigation errors. The control law applies a secular variation of the mean relative argument of latitude in Eq. (19), based upon an atmospheric density $\rho = 0.11946$ g/km^3 and ballistic coefficients $B_M = 0.045$ m^2/kg and $B_T = 0.019$ m^2/kg for Main and Target, respectively. The relative difference of the applied ballistic coefficients corresponds to $\epsilon \approx 140\%$ and is of particular relevance in the simulation.

The simulation models realistic sensors and actuators. A driving factor for the performance of the relative orbit control is the propulsion system's minimum impulse bit (MIB) of 0.7 mm/s, (i.e., the thrusters can only realize delta-V as integer multiples of the MIB). Furthermore, the thruster execution error η is treated as Gaussian noise with 2% mean and a standard deviation of 1%. The performance of the GPS-based relative navigation filter is emulated using errors $\Delta\rho$, consisting of a bias of 0.1 m and Gaussian noise with a standard deviation of 0.05 m. Finally, the attitude control errors $\Delta\alpha$ are accounted for by Gaussian noise with 0.8-deg standard deviation in three axes. This implies a thrust direction misalignment, which causes a cross coupling between tangential and normal maneuvers and introduces unintentional velocity variations in radial direction.

The results for the relative e/i vector control in Fig. 5 can be shown to be similar to the case with ideal sensors and actuators. Although the MIB has only minor impact on the relative e/i vector

control, it severely impacts the mean along-track separation control. Because the MIB corresponds to a differential drag effect of 60 m in mean along-track separation, the presented feedback control law is not able to control the separation at a better level (cf. Figure 6). Thus, as expected, the feedback control law can confine the relative mean along-track separation within, at most, ±60 m from the nominal value (i.e., $a\Delta u^N = 33.1$ m).

For the specific simulation scenario considered, the daily maneuver budget for in-plane control amounts to 0.0133 m/s, whereas the daily maneuver budget for out-of-plane control amounts to 0.0236 m/s. The daily delta-V loss in the radial direction amounts to 0.0003 m/s, which results in an overall daily delta-V budget of 0.0372 m/s for the selected formation flying configuration.

Conclusions

PRISMA is a technology demonstration mission for the in-flight validation of sensor and actuator technologies and of guidance, navigation, and control strategies for in-orbit servicing and spacecraft formation flying. The paper provides an overview of the mission, including mission objectives, mission description, and spacecraft design, with an emphasis on the GPS receiver, the thruster characterization, and the onboard software concept.

PRISMA comprises GPS-based navigation, guidance, and control capabilities for real-time demonstration of completely space-based, closed-loop autonomous formation flying. High-grade GPS receivers will provide raw pseudorange data with 0.5-m accuracy and carrier-phase data with 1-mm accuracy under nominal tracking conditions. An innovative Kalman filter concept was presented that provides absolute position determination with accuracies of better than 2 m and relative position accuracies of 0.1 m. To this end, a single filter design is employed that abandons the separation of absolute and relative states and comprises the absolute state vectors of the two PRISMA spacecraft. Although the absolute spacecraft orbits are derived mainly from pseudorange data, the ambiguity resolution of highly precise double-difference carrier-phase data enables the precise reconstruction of the relative orbit, which is simply realized by subtracting the two absolute state vectors.

A relative orbit control concept for the PRISMA formation flying mission was presented that can maintain a desired osculating relative motion between the spacecraft with minimum thruster usage and minimum collision hazard. The concept applies a parameterization of the relative motion in terms of relative eccentricity/inclination vectors and allows for an intuitive geometrical representation of the formation flying configurations. The impulsive orbit control of relative e/i vectors provides a particularly simple implementation of guidance and control functionalities for autonomous formation flying.

Numerical simulations have uncovered strengths and weaknesses of the adopted impulsive feedback control law. Despite its operational simplicity and its low computational burden, the impulsive orbit control suffers from the limitations given by the thruster system. In particular, the minimum impulse bit was identified as a key factor limiting the relative orbit control accuracy. The in-plane maneuver execution errors caused by a discretization of the thruster burn time are directly transferred into residual secular drifts of the relative mean argument of latitude and can only be compensated by the subsequent tangential maneuvers. The uncertainty resulting in the along-track separation justifies the strategy of relative eccentricity/inclination vector separation to minimize the collision hazard and allow for smaller absolute separations between the spacecraft in the formation. Considering safe operational margins, relative orbit control accuracies below ten meters in radial/cross-track direction allow for minimum separations between the spacecraft of a hundred meters perpendicular to the flight direction.

PRISMA will demonstrate, for the first time in Europe, a GPS-based fully autonomous closed-loop formation flying of spacecraft. This is considered a key milestone for autonomous formation flying and paves the way for advanced formation flying missions in low Earth orbit.

References

[1] Leitner, J., Bauer, F., Folta, D., Carpenter, R., Moreau, M., and How, J., "Formation Flight in Space Distributed Spacecraft Systems Develop New GPS Capabilities," *GPS World*, Vol. 13, No. 2, Feb. 2002, pp. 22–31.

[2] Gonnaud, J. L., Lagarde, L., Strandmoe, S. E., and Ballereau, A., "Relative GPS Navigation Implementation for the ATV Rendezvous," *Proceedings of the 5th ESA Conference on Spacecraft Guidance, Navigation and Control Systems*, ESA, Paris, 2003, pp. 225–232.

[3] Kirschner, M., Montenbruck, O., and Bettadpur, S., "Flight Dynamics Aspects of the GRACE Formation Flying," *Second International Workshop on Satellite Constellations and Formation Flying Proceedings*, Technion—Israel Inst. of Technology, Haifa, Israel, Feb. 2001, pp. 187–194.

[4] Folta, D., and Hawkins, A., "Preliminary Results of NASA's First Autonomous Formation Flying Experiment Earth Observing-1 (EO-1)," NASA Goddard Space Flight Center, Greenbelt, MD, 2001, pp. 1–21.

[5] Stephens, G. L., Vane, D. G., Boain, R. J., Mace, G. G., Sassen, K., Wang, Z., Illingworth, A. J., O'Connor, E. J., Rossow, W. B., Durden, S. L., Miller, S. D., Austin, R. T., Benedetti, A., Mitrescu, C., Folta, D., and Hawkins, A., "The Cloudsat Mission and the A-Train," *Bulletin of the American Meteorological Society*, Vol. 83, No. 12, Dec. 2002, pp. 1771–1790.

[6] "Overview of the DART Mishap Investigation Results" [online NASA release], http://www.nasa.gov/pdf/148072main_DART_mishap_overview.pdf [retrieved 24 May 2006].

[7] Gill, E., and Runge, H., "Tight Formation Flying for an Along-Track SAR Interferometer," *Acta Astronautica*, Vol. 55, Nos. 3–9, 2004, pp. 473–485.

[8] Moreira, A., Krieger, G., Hajnsek, I., Hounam, D., Werner, M., Riegger, S., and Settelmeyer, E., "TanDEM-X: A TerraSAR-X Add-on Satellite for Single-Pass SAR Interferometry," *Proceedings of the International Geoscience and Remote Sensing Symposium*, Vol. 2, Inst. of Electrical and Electronics Engineers, New York, 2004, pp. 1000–1003.

[9] D'Amico, S., and Montenbruck, O., "Proximity Operations of Formation-Flying Spacecraft Using an Eccentricity/Inclination Vector Separation," *Journal of Guidance, Control, and Dynamics*, Vol. 29, No. 3, May–June 2006, pp. 554–563.

[10] Persson, S., Jakobsson, B., and Gill, E., "PRISMA—Demonstration Mission for Advanced Rendezvous and Formation Flying Technologies and Sensors," 56th International Astronautical Congress, Fukuoka, Japan, International Astronautical Congress Paper 05-B56B07, 2005.

[11] Leung, S., and Montenbruck, O., "Real-Time Navigation of Formation-Flying Spacecraft Using Global Positioning System Measurements," *Journal of Guidance, Control, and Dynamics*, Vol. 28, No. 2, Mar.–Apr. 2005, pp. 226–235.

[12] Busse, F. D., How, J. P., and Simpson, J., "Demonstration of Adaptive Extended Kalman Filter for Low-Earth-Orbit Formation Estimation Using CDGPS," *Journal of the Institute of Navigation*, Vol. 50, No. 2, 2003, pp. 79–93.

[13] Hill, G. W., "Researches in the Lunar Theory," *American Journal of Mathematics*, Vol. 1, No. 1, 1878, pp. 5–26.

[14] Clohessy, W., and Wiltshire, R., "Terminal Guidance Systems for Satellite Rendezvous," *Journal of the Aerospace Sciences*, Vol. 27, No. 9, 1960, pp. 653–658.

[15] Schweighart, S., and Sedwick, R., "High-Fidelity Linearized J2 Model for Satellite Formation Flight," *Journal of Guidance, Control, and Dynamics*, Vol. 25, No. 6, 2002, pp. 1073–1080.

[16] Schaub, H., and Alfriend, K. T., "J2 Invariant Relative Orbits for Spacecraft Formations," *1999 Flight Mechanics Symposium*, CP-1999-209235, NASA Goddard Space Flight Center, Greenbelt, MD, May 1999, pp. 125–139.

[17] Eckstein, M. C., Rajasingh, C. K., and Blumer, P., "Colocation Strategy and Collision Avoidance for the Geostationary Satellites at 19 Degrees West," *Mécanique Spatiale*, Colloque, Cepadues Editions, Toulouse, France, Nov. 1989, pp. 85–97.

[18] Montenbruck, O., Kirschner, M., D'Amico, S., and Bettadpur, S., "E/I-Vector Separation for Safe Switching of the GRACE Formation," *Aerospace Science and Technology*, Vol. 10, No. 7, 2006, pp. 628–635.

[19] Brouwer, D., "Solution of the Problem of Artificial Satellite Theory Without Drag," *Astronomical Journal*, Vol. 64, No. 1274, 1959, pp. 378–397.

[20] Lyddane, R. H., "Small Eccentricities or Inclinations in the Brouwer Theory of the Artificial Satellite," *Astronomical Journal*, Vol. 68, No. 8, 1963, pp. 555–558.

[21] Micheau, P., "Orbit Control Techniques for Low Earth Orbiting (LEO) Satellites," *Spaceflight Dynamics*, Cepadues Editions, Toulouse, France, 1995, pp. 739–902.

[22] Montenbruck, O., and Markgraf, M., "User's Manual for the Phoenix GPS Receiver, Ver. 1.6," DLR, German Aerospace Center, GTN-MAN-0120, Oberpfaffenhofen, Germany, June 2005.

[23] Anflo, K., "PRISMA HPGP Reaction Control System Specification," Ecological Advanced Propulsion Systems (ECAPS), Rept. SPS-TS-1009ECAPS, Solna, Sweden, 2005.

[24] Gaisler, J., "The LEON Processor User's Manual Ver. 2.3.7," Gaisler Research, Goteborg, Sweden, 2001.

[25] Hofmann-Wellenhof, B., Lichtenegger, H., and Collins, J., *Global Positioning System Theory and Applications*, Springer, New York, 1997.

[26] Yunck, T. P., "Coping with the Atmosphere and Ionosphere in Precise Satellite and Ground Positioning," *Environmental Effects on Spacecraft Positioning and Trajectories*, Vol. 13, Geophysical Monograph 73, International Union of Geodesy and Geophysics and the American Geophysical Union, Washington, D.C., 1993, pp. 1–16.

[27] Gill, E., and Montenbruck, O., "Comparison of GPS-based Orbit Determination Strategies," *Proceedings of the 18th International Symposium on Space Flight Dynamics*, SP-548, ESA, Noordwijk, The Netherlands, 2004, pp. 169–174.

[28] Montenbruck, O., and Gill, E., *Satellite Orbits—Models, Methods and Applications*, Springer, Heidelberg, Germany, 2000, pp. 53–116.

[29] Montenbruck, O., and Gill, E., "State Interpolation for On-Board Navigation Systems," *Aerospace Science and Technology*, Vol. 5, No. 3, 2001, pp. 209–220.

[30] Gill, E., and Runge, H., "A Tight Formation for Along-Track SAR Interferometry," *2nd International Symposium on Formation Flying Missions & Technologies* [CD-ROM], CP-2005-212781, NASA Goddard Space Flight Center, Greenbelt, MD, 2004.

[31] Richardson, D. L., and Mitchell, J. W., "A Third-Order Analytical Solution for Relative Motion with a Circular Reference Orbit," *Journal of the Astronautical Sciences*, Vol. 51, No. 1, 2003, pp. 1–12.

[32] Vaddi, S. S., Alfriend, K. T., Vadali, S. R., and Sengupta, P., "Formation Establishment and Reconfiguration Using Impulsive Control," *Journal of Guidance, Control, and Dynamics*, Vol. 28, No. 2, 2005, pp. 262–268.

C. McLaughlin
Associate Editor